J Solid State Electrochem (2012) 16:2661–2666
DOI 10.1007/s10008-012-1692-9

ORIGINAL PAPER

Highly stable performance of supercapacitors using microporous carbon derived from phenol–melamine–formaldehyde resin

Xiaoxia Xiang · Enhui Liu · Hui Xie · Yingying Tian · Yuhu Wu · Zhilian Wu · Yinhai Zhu

Received: 23 December 2011 / Revised: 10 February 2012 / Accepted: 13 February 2012 / Published online: 28 February 2012

Abstract A series of microporous carbons were prepared by simple carbonization and activation of phenol–melamine–formaldehyde resin. The morphology, surface area, and elemental composition of the samples were investigated by scanning electron microscope, Brunauer–Emmett–Teller measurement, Raman spectra, and elemental analysis, respectively. Electrochemical characteristics were evaluated by cyclic voltammograms, galvanostatic charge/discharge, and electrochemical impedance spectroscopy measurements in 6.0 mol L^{-1} KOH. The microporous carbon activated by KOH presented a high specific capacitance of 202 $F g^{-1}$ at a scan rate of 2 mV s^{-1}. Furthermore, the KOH-activated microporous carbon electrode exhibited durable operation, the total loss of capacitance after 20,000 cycles is 2% at a current density of 500 mA g^{-1}. The good electrochemical performance of the activated carbon was ascribed to well-developed micropores, high surface area, larger pore volume as well as oxygen groups.

Keywords Supercapacitors · Microporous carbon · Polymer · Electrochemical properties

Introduction

Supercapacitor (also called electrochemical capacitors), as energy storage devices with high power density and long cycle life, have been considered to be a promising high power energy source for hybrid electrical vehicles, digital telecommunication systems, and so on [1–4]. Usually, supercapacitors may be divided into two categories, namely, electrical double-layer capacitors (EDLCs) and pseudocapacitors, which are distinguished by their charge storage mechanisms [4, 5]. EDLCs show an electrostatic attraction with accumulation of charges at the electrode/electrolyte double-layer interfaces. In contrast, a pseudocapacitor uses a conducting polymer [6] or transition metal oxides [7] as an electrode material, which undergoes reversible faradic redox reactions at or near the electrode surface.

In recent years, much effort has been focused on developing better supercapacitor electrode materials. Up to date, activated carbon is well known as promising materials for future capacitors due to their well-developed microstructure, high surface area, electrochemical stability, good conductivity, and low cost [8–10]. Their porosity, mainly micro- and mesoporous, allows an easy penetration of the electrolyte species and easy access to the smallest pores. Particularly, the abundant micropores play an essential role for optimizing the electrical double-layer surfaces and then strengthen the value of capacitance. Moreover, their porosity can be significantly developed by activation: physically with steam or carbon dioxide, or chemically with chemical reagents, i.e., KOH, K_2CO_3, $ZnCl_2$, and H_3PO_4 [11–14]. Generally, chemical activation is the preferred route because it achieves higher yield, larger surface area, needs low operating temperature, less activation time, and is cost-effective.

Various activated carbons derived from phenolic resin such as phenol–formaldehyde resin [15–17], resorcinol–formaldehyde resin [18–20], pyrocatechol–formmaldehyde resin [21], and melamine–formaldehyde [22, 23] have been reported. Herein, a serial of oxygen-rich microporous carbons with high specific surface area were prepared from

Electronic supplementary material The online version of this article (doi:10.1007/s10008-012-1692-9) contains supplementary material, which is available to authorized users.

X. Xiang · E. Liu (✉) · H. Xie · Y. Tian · Y. Wu · Z. Wu · Y. Zhu
Key Laboratory of Environmentally Friendly Chemistry and Applications of Ministry of Education, College of Chemistry, Xiangtan University,
Hunan 411105, People's Republic of China
e-mail: liuenhui99@sina.com.cn

phenol–melamine–formaldehyde (PMF) resin by chemical activation. We present an easy-accessed method by directly mixing phenol, melamine, and formaldehyde under designed aqueous basic/acidic conditions (first weakly basic condition then highly acidic condition) to synthesis well-developed microporous carbon, which could overcome the restriction of the narrow pH range and simplify the synthesis procedures. Though activated carbon has been prepared from PMF gels [24], the synthesis route was different with ours, and we have used PMF resin-based-activated carbons as electrode materials for supercapacitors, which presented good electrochemical properties.

Experimental

Preparation of PMF resin

All reagents used were of analytical grade, and distilled water was used in this experiment. Melamine (11.7 g), 37% formaldehyde solution (32.6 g) and triethylamine (6.3 g) were dissolved in 150 ml distilled water to form a homogeneous mixture with the pH value is about 9. The mixture was heated to 75 °C under vigorous stirring. After 30 min, phenol (64.6 g) was slowly added to the mixture. After stirring for 15 min and then 85% H_3PO_4 solution (14.8 g) was added to decrease the pH value to about 3. After stirring for another 12 h at 75 °C, the resulting buff powder was filtered, washed, and dried at 100 °C for 48 h to obtain the PMF resin.

Preparation of carbon materials

The PMF resin were mixed for 4 h with 1:2 weight ratio of chemical reagents, i.e., K_2CO_3, KOH, and $ZnCl_2$ dissolved in a small amount of distilled water. After drying at 110 °C for 24 h, the mixture were heated to 700 °C or 800 °C at a heating rate of 5 °C min^{-1} under nitrogen flow and maintained at the desired temperature for 1 h. The as-prepared products were washed with distilled water and then dried at 110 °C for 24 h. In order to facilitate the description in the text, the activated samples using K_2CO_3, KOH, $ZnCl_2$ as chemical reagents were marked as AKC800, AKH800, and AZ700, respectively. For comparison, a carbonized sample from PMF resin at 700 °C under nitrogen is marked as C700.

Characterization and measurements

Scanning electron microscope (SEM) measurements were performed on a JEOL JEM-3010. The Brunauer–Emmett–Teller (BET) specific surface area of the carbon materials were determined by N_2 adsorption at 77 K on a Quantachrome NOVA-2200 system. The pore size distributions were estimated by density functional theory (DFT) method. Raman spectra were recorded on a Jobin-Yavon U-1000 micro-Raman system at room temperature at an excitation wavelength of 532 nm. The elemental analyses were performed on an elemental analyzer Vario EL V5 (Elementar analysensysteme GmbH).

Electrochemical testing

The electrode was prepared by mixing the obtained carbon (80%), acetylene black (10%), and polyvinylidene fluoride (10%) in *N*-methylpyrrolidone to form a homogenous slurry. The slurry was then spread onto a nickel foam and dried at 100 °C for 24 h in a vacuum oven. Sandwich-type capacitors were assembled with two electrodes separated by nylon film, and 6 mol L^{-1} KOH solution was used as electrolyte. Cyclic voltammetry (CV), galvanostatic charge/discharge cycles, and electrochemical impedance spectroscopy (EIS) were conducted on a CHI 660A electrochemical workstation (CHI Inc., USA) at room temperature. EIS measurements were carried out by applying an AC voltage of 5 mV amplitude in the 100 kHz to 10 mHz frequency range. The cycling performance was charged and discharged in the potential range of 0.001–1.0 V at a constant current density of 500 mA g^{-1} on a Neware BTS cell test apparatus. In addition, the influence of the binder (5–15%) on the electrochemical properties of the active material were not obvious (Electronic supplementary material (ESM) Fig. S1).

Results and discussion

The SEM images of the as-prepared samples are presents microbead shapes (ESM Fig. S2).

Typical nitrogen adsorption/desorption isotherms of the as-prepared samples are shown in Fig. 1a. In the isotherm of C700, the adsorbed volume is very small, indicating its nonporous characteristics. In the isotherms of AKC800, AKH800, and AZ700, according to the International Union of Pure and Applied Chemistry classification, the N_2 adsorption isotherms exhibit type I characteristics, indicating their microporous features. Figure 1b denotes the corresponding pore size distribution curves by the DFT method of the as-prepared samples. It is seen in Fig. 1b that the adsorbed volume of C700 is very small, indicating its nonporous characteristics. As for AKC800, AKH800, and AZ700, relatively sharp peaks at pore diameter less than 2 nm indicate the formation of micropores. Meanwhile, it is also noticeable that peaks are exhibited in the pore size range of 2–4 nm for AKH800, which confirms that AKH800 contain both micropores and mesopores.

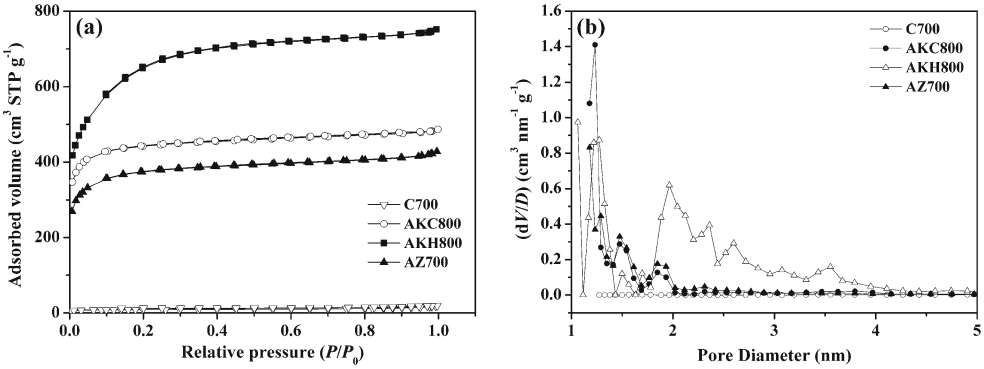

Fig. 1 Nitrogen adsorption/desorption isotherms and the DFT pore size distributions of the as-prepared samples

The textural properties of the as-prepared samples are summarized in Table 1. The BET surface area, micropore surface area, and total pore volume of the porous carbons increase remarkably after chemical activation. AKH800 exhibits the highest BET surface area of 2,376 $m^2\ g^{-1}$ and a total pore volume of 1.07 $cm^3\ g^{-1}$. At the same time, a steady increase of micropore volume could be found for these carbons. As a result, the average pore diameter decreased after activation.

Figure 2 shows the first-order Raman spectrum of the as-prepared carbons. The first-order spectrum of carbons exhibit two broad and strongly overlapping peaks. The peak at ~1,350 cm^{-1} (disorder-induced D band) is attributed to A_{1g} model and is associated with the presence of structural defects and disorders of carbon materials, while the peak at ~1,600 cm^{-1} (G band) has E_{2g} symmetry and is related to the vibration of sp^2-bonded carbon atoms in a two-dimensional hexagonal lattice, resulting from the stretching modes of C=C bonds of typical graphite [25–27]. It is worth noting that the peak positions of G- and D-band shift to a higher wavelength number in comparison with that of single crystal, suggesting a structural imperfection of the graphene sheets of material [28]. However, the width and intensity of these two peaks suggest the disordered nature of the as-prepared carbons. In addition, the relative intensity of D- against G-band also represents the degree of disorder in the graphite structure. It can be seen in Fig. 3 that the values of full width at half maximum of D- and G-band stay approximately constant or decrease only slightly after activation, and the ratio of the integrated intensities of the D- and G-bands (I_D/I_G) of the as-prepared carbond are almost the same (I_D/I_G=0.99–1.01), indicating no significant change in overall graphite structure after activation.

Elemental analyses of the as-prepared samples are also shown in Table 1. After activation, the high oxygen content of 7.3%, 10.7%, and 11.5% were retained in AKH800, AKC800, and AZ700, respectively. As a result of self-oxidation, the carbon surface is usually decorated with oxygen functional groups such as quinone, which can enhance the capacitance of porous carbon by enhancing the carbon wettability and by pseudo-Faradaic reactions [29–31].

Typical CV curves for the nickel foam and as-prepared carbons at a scan rate of 2 mV s^{-1} are presented in Fig. 3a. It can be observed that all the carbons present a quasirectangular voltammogram shape at the low scan rate. Particularly, the AKC800 and AKH800 give similar high specific capacitance, which is due to their high surface area, well-developed micropores, and the presence of oxygen groups. Moreover, the capacitance contribution of nickel foam could be ignored. Figure 3b presents the CV curves for activated carbons at a scan rate of 100 mV s^{-1}. The activated carbons still show a quasirectangular voltammogram shape at the high scan rate indicative of a good candidate as electrode materials for supercapacitors.

Figure 4 shows the variation of specific capacitances at different scan rates. The specific capacitances of all samples decrease as the scan rate increase. This confirms that at the low currents, the ions have enough time to diffuse into the micropores of carbons; while at the high currents, the ions can only partially penetrate into the micropores due to the sterical limitations [9, 32]. However, the specific capacitance of

Table 1 Textural characteristics, elemental analysis (carbon, hydrogen, nitrogen, and oxygen contents [%]), and specific capacitance (test at a scan rate of 2 mV s^{-1}) of the as-prepared samples

Samples	BET	S_{mic}	V_t	V_{mic}	D	Elemental analysis				C_{spec}
	$m^2\ g^{-1}$	$m^2\ g^{-1}$	$cm^3\ g^{-1}$	$cm^3\ g^{-1}$	nm	C	H	N	O	$F\ g^{-1}$
C700	30.6	–	0.03	–	3.75	76.7	1.4	9.4	12.5	58
AKC800	1,610	1,485	0.63	0.51	1.07	87.4	0.4	1.5	10.7	208
AKH800	2,376	1,934	1.07	0.83	1.42	90.8	0.4	1.5	7.3	202
AZ700	1,296	1,164	0.54	0.52	0.95	79.7	1.0	7.8	11.5	153

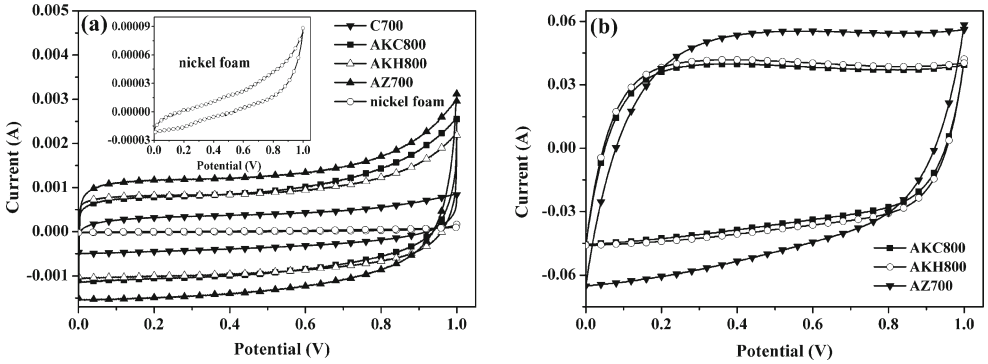

Fig. 2 Raman spectra of the as-prepared samples

AKH800, AKC800 and AZ700 can still remain as high as 178, 173, and 122 Fg^{-1} at the high scan rate of 100 mV s^{-1}, 88.3%, 83.4%, and 80% of that measured at 2 mV s^{-1}, respectively. It suggests that, after activation, more surface area of the carbons was accessible to electrolyte ions due to the improved wettability of the carbon and faster charge propagation [33]. This result is supported by BET results.

Galvanostatic charge/discharge measurements are commonly used to test the performance of capacitors. Galvanostatic charge/discharge curves of the samples at the current density of 500 mA g^{-1} between 0 and 1.0 V in a 6.0 mol L^{-1} KOH electrolyte are shown in Fig. 5. The galvanostatic charge/discharge curves of the samples exhibit almost the isosceles triangle curves, with low IR drops, which indicate the supercapacitors with the performance of electrochemical stability and reversibility. However, the specific capacitance of AKC800, AKH800 and AZ700 reach 188, 190, and 140 Fg^{-1}, respectively, much larger than that of the C700 (53 Fg^{-1}). The specific capacitance of the samples was calculated from the discharge side of the galvanostatic charge/discharge profiles. In addition, although the AKC800 and AKH800 give similar specific capacitance, the efficiency of charge/discharge of AKH800 (97.2%) is larger than AKC800 (85.7%), which may be ascribed to its abundant micropore volume and suitable average pore size, as the average pore size of AKH800 is large enough to allow the fast access of the ions compared.

The Ragone plots are frequently used in demonstration of power densities and energy densities of supercapacitors and Fig. 6 displays the plots for AKC800, AKH800, and AZ700. The energy and power densities are calculated from the galvanostatic cycling of a supercapacitor charged up to 1.0 V at current densities from 0.5 to 5A g^{-1}. The highest energy densities are obtained from AKH800. As the power density increased from 1,000 to 8,800 Wkg^{-1}, the energy density of AKH800 dropped from 26.3 to 20.7 Wh kg^{-1}. The other carbons show similar trends. The energy and power limitations normally observed at high rates are associated with the tortuous diffusion pathways within the porous textures. At high discharge current, only some parts of the pores can be accessed by the ions; whereas at low current, total surfaces are used for charge storage. The good energy and power performances of porous carbons (typically AKH800) confirm that most of micropores skeleton can be effectively utilized for charge storage.

The cyclability of activated carbon electrodes are tested by continuous galvanostatic charge/discharge to 20,000

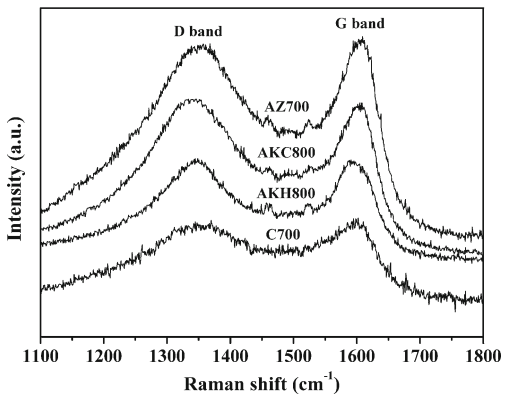

Fig. 3 Cyclic voltammograms of the electrode materials in 6 mol L^{-1} KOH aqueous electrolyte: **a** as-prepared samples and nickel foam at a scan rate of 2 mV s^{-1} (*inset* enlarged CV curve of nickel foam), **b** activated carbons at a scan rate of 100 mV s^{-1}. The weight of nickel foam is 65 mg, while the weight of electroactive material in each electrode for C700, AKC800, AKH800, and AZ700 is 6.24, 4.48, 4.48, and 8.56 mg, respectively

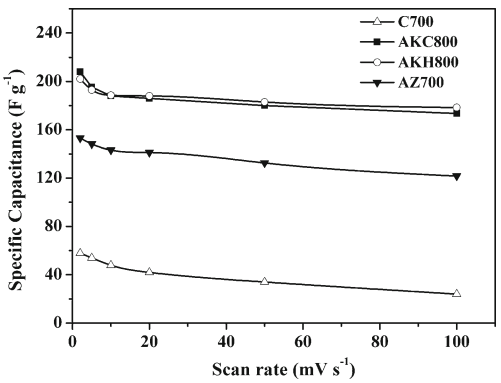

Fig. 4 Specific capacitance of the as-prepared samples as a function of scan rate

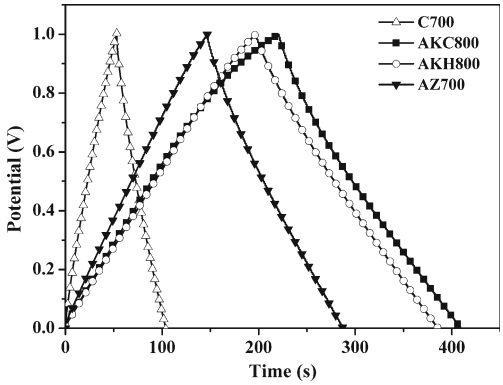

Fig. 5 Galvanostatic charge/discharge curves of the as-prepared samples

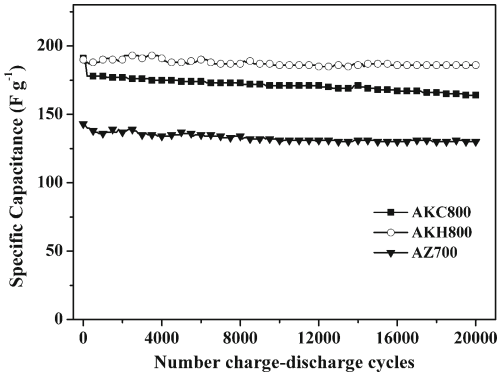

Fig. 7 Cycle performance of the activated carbon electrodes at a current density of 500 mA g^{-1}

cycles (see Fig. 7) at a current density of 500 mA g^{-1}. A little decrease of specific capacitance mainly occurs at the initial 2,000 cycles, and thereafter the specific capacitance tends to stabilize. After 20,000 cycles, the specific capacitance of AKH800 is still about 98% of the initial specific capacitance, which can be ascribed to its high surface area and well-developed micropores. The particular stability of AKH800 may also be explained by the existence of lower oxygen groups such as quinone, which are electrochemically active but not stable and can cause capacitance deterioration. This is also supported by the high specific capacitance of AKC800 but with a poorest cycling performance among the three activated carbons. At the same time, the specific capacitance drop of AZ700 can result from the high oxygen content, and the pore size of <1 nm limiting the accessibility to the surface with cycling.

The resistance of a supercapacitor, namely equivalent series resistance or ESR, consists of electronic resistance and ionic resistance. Typical Nyquist impedance spectra the as-prepared samples are shown in Fig. 8. At very high frequencies, the intercept at the real axis is the ESR value. It can be seen that the ESR of the activated carbons, particularly, the AKH800 (1.3 Ω) is lower than that of C700 (1.8 Ω), indicating that the electric conductivity increases.

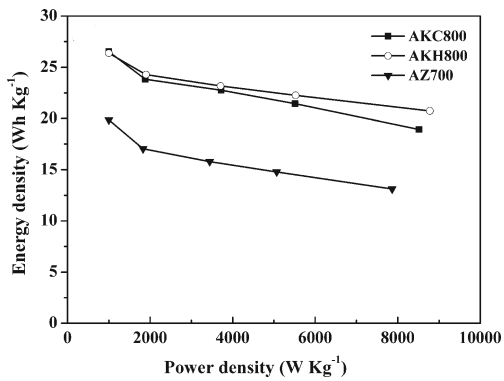

Fig. 6 Ragone plots of the AKC800, AKH800, and AZ700

The lower electronic resistance for activated carbons is probably attributable to more rapid mass transport within micropores of carbon due to the improved wettability of active material [34]. In addition, the straight line in all plots in the low-frequency region reveals the capacitive nature of the carbons. The slopes of microporous carbons are steeper than that of C700, which suggests that the capacitive performance is better than that of C700. This is consistent with above results from CV curves.

Conclusions

Microporous carbons with high surface area were prepared from PMF resin by simple carbonization and activation. Various chemical reagents such as K_2CO_3, KOH, and $ZnCl_2$ were used for activating. Owing to their high surface area, large amount of micropores less than 1.5 nm, disorder structure, high oxygen-containing, and low ESR, the obtained carbon materials cherishes good electrochemical performance such as high specific capacitance, high energy and power densities, and cycling stability.

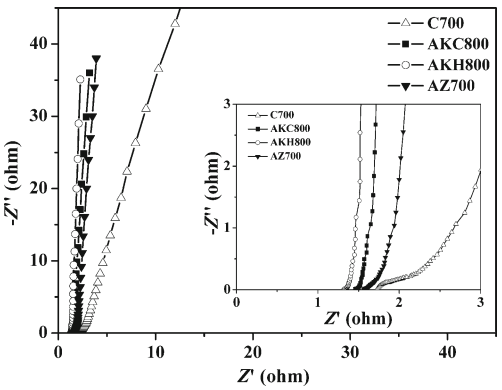

Fig. 8 Nyquist plot of the as-prepared samples (*inset* enlarged high-frequency region of Nyquist plot)

Acknowledgments The authors are grateful for the project support by National Natural Science Foundation of China (51172190) and Hunan Provincial Natural Science Foundation of China (11JJ2030).

References

1. Wu DC, Chen X, Lu SH, Liang YR, Xu F, Fu RW (2010) Microporous Mesoporous Mater 131:261–264
2. Algharaibeh Z, Pickup PG (2011) Electrochem Commun 13:147–149
3. Yang XQ, Wu DC, Chen XM, Fu RW (2010) J Phys Chem C 114:8581–8586
4. Du QL, Zheng MB, Zhang LF, Wang YW, Chen JH, Xue LP, Dai WJ, Ji GB, Cao JM (2010) Electrochim Acta 55:3897–3903
5. Ruiz V, Santamaría R, Granda M, Blanco C (2009) Electrochim Acta 54:4481–4486
6. Liu CG, Yu ZN, Neff D, Zhamu A, Jiang BZ (2010) Nano Lett 10:4863–4868
7. Sharma RK, Rastogi AC, Desu SB (2008) Electrochem Commun 10:268–272
8. Li XL, Han CL, Chen XY, Shi CW (2010) Microporous Mesoporous Mater 131:303–309
9. Xing W, Huang CC, Zhuo SP, Yuan X, Wang GQ, Hulicova-Jurcakovac D, Yan ZF, Lu GQ (2009) Carbon 47:1715–1722
10. Lin JH, Ko TH, Lin YH, Pan CK (2009) Energy Fuel 23:4668–4677
11. Xiang XX, Liu EH, Li LM, Yang YJ, Shen HJ, Huang ZZ, Tian YY (2011) J Solid State Electrochem 15:579–585
12. Niu HT, Zhang J, Xie ZL, Wang XG, Lin T (2011) Carbon 49:2380–2388
13. Ruiz V, Pandolfo AG (2010) Electrochim Acta 55:7495–7500
14. Jiang JH, Gao QM, Xia KS, Hu J (2009) Microporous Mesoporous Mater 118:28–34
15. Huang CH, Doong RA (2012) Microporous Mesoporous Mater 147:47–52
16. Szczurek A, Jurewicz K, Amaral-Labat G, Fierro V, Pizzi A, Celzard A (2010) Carbon 48:3874–3883
17. Xie MJ, Dong HH, Zhang DD, Guo XF, Ding WP (2011) Carbon 49:2459–2464
18. Halama A, Szubzda B, Pasciak G (2010) Electrochim Acta 55:7501–7505
19. Wen ZB, Qu QT, Gao Q, Zheng XW, Hu ZH, Wu YP, Liu YF, Wang XJ (2009) Electrochem Commun 11:715–718
20. Górka J, Jaroniec M (2011) Carbon 49:154–160
21. Moreno-Castilla C, Dawidziuk MB, Carrasco-Marín F, Zapata-Benabithe Z (2011) Carbon 49:3808–3819
22. Dong YR, Nishiyama N, Kodama M, Egashira Y, Ueyama K (2009) Carbon 47:2138–2141
23. Hulicova D, Yamashita J, Soneda Y, Hatori H, Kodama M (2005) Chem Mater 17:1241–1247
24. Long DH, Zhang J, Yang JH, Hu ZJ, Cheng G, Liu XM, Zhang R, Zhan L, Qiao WM, Ling LC (2008) Carbon 46:1253–1269
25. Ji LW, Zhang XW (2009) Electrochem Commun 11:684–687
26. Chun KY, Lee HS, Lee CJ (2009) Carbon 47:169–177
27. Jänes A, Kurig H, Lust E (2007) Carbon 45:1226–1233
28. Zhang GQ, Zhang ST (2009) J Solid State Electrochem 13:887–893
29. Seredych M, Hulicova-Jurcakova D, Lu GQ, Bandosz TJ (2008) Carbon 46:1475–1488
30. Hulicova-Jurcakova D, Seredych M, Lu GQ, Bandosz TJ (2009) Adv Funct Mater 19:438–447
31. Kalpana D, Karthikeyan K, Renganathan NG, Lee YS (2008) Electrochem Commun 10:977–979
32. Pandolfo AG, Hollenkamp AF (2006) J Power Sources 157:11–27
33. Fang BZ, Binde L (2006) J Phys Chem B 110:7877–7882
34. Xiang XX, Liu EH, Huang ZZ, Shen HJ, Tian YY, Xiao CY, Yang JJ, Mao ZH (2011) J Solid State Electrochem 15:2667–2674